Influence of Absolute Pressure of H_2/H_2O on Corrosion of Ferritic Stainless Steel at 850 °C

Patrik Alnegren*[a], Swathi Kiranmayee Manchili [b], Jan-Erik Svensson[a], Jan Froitzheim [a]

a) Energy and Materials, Chemistry and Chemical Engineering, Chalmers University of Technology

b) Materials and Manufacture, Industrial and Materials Science, Chalmers University of Technology

Kemivägen 10, 41296 Gothenburg, Sweden

*Corresponding author. Tel.: +46 31 772 2828; fax: +46 31 772 2853;
E-mail address: patrik.alnegren@chalmers.se
Kemivägen 10, 41296 Gothenburg, Sweden

1 Abstract

Ferritic stainless steel interconnects must be able to withstand high contents of steam on the fuel side of solid oxide electrolysis cells (SOEC) and on solid oxide fuel cells (SOFC) that run high fuel utilization. SOEC fuel environment is often simulated by diluting mixtures H_2O/H_2 with inert gas due to safety restrictions on handling hydrogen. The current study investigates the influence of the absolute pressure of H_2O/H_2 at a constant pO_2 using different levels of dilution with Ar on the corrosion behavior of the ferritic stainless steels AISI 441 and Crofer 22 APU up to 500 h. It is shown that Crofer 22 APU has the same oxidation rate regardless of the absolute pressure of H_2/H_2O, but the lower alloyed AISI 441 oxidizes rapidly due to iron-rich oxide formation when the water content is increased to 40%.

2 Introduction

Ferritic stainless steels are used as interconnects in solid oxide fuel cells and electrolyzers (SOFC and SOEC), where they electrically connect stacked cells and separate the oxidant and fuel gases. The formation of chromia scales provides protection against rapid oxidation of the interconnects, and chromia is considered sufficiently electrically conductive at operating temperatures of around 600-900 °C, as opposed to silica or alumina scales [1,2]. The interconnects can be exposed to high concentrations of steam on the fuel facing side, especially in the case of steam electrolysis [3]. The presence of water vapor is known to accelerate oxidation and promote break-away corrosion, i.e. the formation of rapid-growing Fe oxide on stainless steels [4]. To form a continuous protective chromia scale on a steel, the flux of C from the alloy towards the metal/oxide interface must exceed that of the inward flux of oxygen ions [5]. Or in other terms, the supply of Cr must be larger than the consumption, otherwise Fe-rich oxide, which has a higher concentration of defects, will form, which leads to much faster oxidation.

This makes the oxidation of stainless steels rather complex. It is interesting to consider first alloys that form chromia as the only oxide scale. Hultqvist et al. have shown that pure chromium oxidizes faster in

H_2O than in O_2 at 900 °C [6]. Hänsel et al. have studied the oxidation of pure chromium at 1 000 °C and concluded that the oxidation rate increases in the presence of water vapor but only at low pressures of oxygen, i.e. in pure steam or mixtures of steam and hydrogen [7]. Accelerated oxidation in the presence of water vapor has also been reported on Fe and Ni base alloys, even though a protective chromia layer had been formed [8,9]. This indicates that the defect chemistry of chromia changes in the presence of water vapor and/or at low partial pressure of oxygen. Chromia is considered to be an extrinsic p-type conductor at temperatures below 1000 °C, but it is reported to change to an n-type conductor at oxygen pressures close to its dissociation pressure [10,11]. Therefore, both of n-type and p-type can behavior can occur in a thermally grown chromia due to the pO_2 gradient over the scale. Galerie et al. have also shown that the thermally grown chromia scale exhibits exclusively n-type behavior when chromium or ferritic steel is exposed to water vapor at 900 °C. Holt and Kofstad have observed that the defect chemistry of pure chromia changes when the absolute pressure of hydrogen is varied at a constant pO_2 [12]. Furthermore, Guillou et al. have exposed the ferritic steel AISI 441 at 800 °C and measured ten times higher electrical conductivity of the scales formed in air than in Ar–1 %H_2–9 %H_2O. This indicates a change in defect chemistry when the atmosphere is changed to humid hydrogen.

Hultquist et al. [6] have suggested that the increased ionic conductivity of chromia is due to the incorporation of interstitial hydrogen during the dissociation of water vapor, which increases the concentration of Cr vacancies. Those authors reported a change to more outward growth of the oxide in water vapor, which they attributed to this hydrogen doping effect. Another mechanism has been suggested by Galerie et al. In this mechanism, the smaller radius of OH^- compared to O^{2-}, in combination with more oxygen vacancies (indicated by a change to n-type conductor), allows for faster inward diffusion of oxygen and a change to a predominantly inward growth of the oxide [11]. Several studies have shown a change from outward growing oxide in air to inward growing oxide in pure H_2O or in H_2/H_2O [8,13,14]. Another aspect to consider is the microstructure of the oxide. Diffusion in chromia, at the useful temperature interval of chromia-forming alloys, has been shown to occur mainly through grain boundary transport [15]. It has been shown that the chromia formed in H_2/H_2O environments has smaller grain structure than chromia formed in air, which could explain the more rapid oxidation observed by some authors [8].

It has been shown that higher contents of Cr are required to form protective chromia scales in FeCr alloys in the presence of water than in atmospheres of air [4]. The increased ionic conductivity due to a change in the defect structure and/or faster diffusing hydroxides requires a higher flux of Cr from the alloy to make up for the faster oxidation and to avoid the oxidation of Fe. An additional hypothesis has been presented by Essuman et al. after observing the internal oxidation of Cr in Fe-Cr alloys exposed to Ar-H_2O and H_2/H_2O at 900 °C. Those authors propose that the dissolution of hydrogen in the alloy causes increased oxygen flux, resulting in Cr being oxidized and tied up inside the alloy, thus reducing the outward flux of Cr towards the metal/oxide interface.

Both the pO_2 and the presence of hydrogen seem to affect the defect chemistry of chromia. However, the pO_2 seem to have a rather weak influence on the oxidation rate of thermally grown chromia [16–19]. In a low- pO_2 environment Hänsel et al. have shown that the oxidation rate of pure chromium increased when the absolute pressure of hydrogen and water vapor was increased, but the pO_2 remained constant. Consequently, it is of interest to further investigate the influence of the absolute pressure of H_2/H_2O on the corrosion of ferritic stainless steels, since their durability relies on the formation of a protective chromia scale. Furthermore, safety restrictions when handling high concentrations of hydrogen, often lead to experiments being carried out by dilution with inert gas, like Ar or N_2, keeping the ratio of H_2/H_2O the same as for the intended simulated environment. This might not always be a representative test environment. In the current study, two commercial ferritic stainless steels are exposed to simulated SOFC/SOEC fuel side gases with different absolute pressures of H_2/H_2O. The higher alloyed Crofer 22

APU is compared to the cheaper AISI 441. We aimed to study the role of water vapor at constant pO_2 as well as to test the possibility of using the investigated materials as interconnects in SOC.

3 Experimental

The materials studied were Crofer APU and AISI 441, both ferritic stainless steels. Their compositions can be found in Table 1. Steel sheets with 0.3 mm thickness were cut into 15x15 mm^2 specimens that were then cleaned with ultra-sonic agitation in acetone and ethanol.

Table 1. Composition of the investigated steels in weight%. The compositions were given by the manufacturers for the received batches.

Steel	Cr	Mn	Ti	Nb	Si	Ni	C	N	S	P	Al	La
AISI 441	17.56	0.35	0.173	0.39	0.59	0.26	0.014	0.017	0.001	0.03	-	-
CROFER 22 APU	22.2	0.46	0.06	-	0.03	0.02	0.005		0.02	0.016	0.02	0.06

Exposures of the materials were carried out in simulated interconnect fuel side conditions inside a horizontal tubular furnace (Al_2O_3 tube) with an inner diameter of 46 mm. A gas mixture of Ar - 5 % H_2 was bubbled through a humidifier set at 80 °C and equilibrated with a coil condenser set at the temperature of 76.4 °C, which resulted in the gas composition of Ar- 40% H_2O- 3% H_2 that was used in one of the experiments. In order to reduce pH_2 and pH_2O but to keep pH_2/pH_2O constant, the humidified gas was diluted with Ar to achieve gas compositions of Ar- 1.5% H_2- 20% H_2O and Ar- 0.75% H_2- 10% H_2O. These environments will hereinafter be referred to as 10% H_2O, 20% H_2O, and 40% H_2O for the purpose of simplicity. The gas compositions and flow rates used in the experiments are summarized in Table 2. The furnace temperature was 850 °C, and the total gas flow rate was 250 smL min^{-1} in all experiments, which corresponds to a mean flow velocity of 1.0 cm s^{-1} inside the reaction chamber. The gas tube that connects the condenser and reaction chamber was heated above 100 °C with a heating cord to ensure that no condensation occurred. An Optidew Vision Precision Dew-Point Hygrometer (chilled mirror) was used to safeguard correct water content.

Exposures were carried out in discontinuous fashion, which means that the furnace was cooled down to room temperature before each gravimetric measurement, and the samples were placed back in the furnace to continue the experiment. The reactor tube was flushed with dry Ar– 5 % H_2 for at least 20 min at 2000 smL min^{-1} before the experiments were resumed. A heating rate of 2.5 °C min^{-1} was employed and natural cooling of the furnace resulted in a lower rate compared to heating. After exposure, the specimens were subjected to gravimetric analysis using a Mettler Toledo XP6 balance. The difference in mass gain before and after exposure was calculated. Samples were removed after 24 h, 72 h, 168 h, and 500 h.

Table 2. The gas composition of the experiments.

Water content in atmosphere	Atmosphere employed	Exposure (Number of hours exposed)
40%	250 ml min^{-1} of 5% H_2-Ar with 40% H_2O	24, 72, 168, 500
20%	125 ml min^{-1} of 5% H_2-Ar with 40% H_2O	24, 72, 168, 500
10%	75 ml/min of 5% H_2-Ar with 40% H_2O	24, 72, 168, 500

Plan view and cross section images of the samples, as well as compositional information, were obtained using scanning electron microscopy with a FEI Quanta FEG 200 ESEM and a Zeiss LEO ULTRA 55 FEG-SEM, both equipped with an INCA X-Sight energy-dispersive X-ray spectroscopy (EDX) system. Cross sections of samples were prepared both by polishing epoxy mounted samples as well as by broad ion beam milling (BIB) with a Leica EM TIC 3X instrument. Grazing incidence X-ray diffraction was performed on the oxide scales of the exposed samples with a Siemens D5000 diffractometer.

4 Results

The mass gain data from all experiments are plotted in the graph in Figure 2. The oxidation rate for Crofer 22 APU was the same regardless of the water concentration. In 10% and 20% H_2O, the oxidation rate for AISI 441 was the same as for Crofer 22 APU. However, in 40% H_2O, AISI 441 had a much higher mass gain after 24h, with an average of 0.38 mg cm^{-2} compared to 0.14 mg cm^{-2} in 10% and 20% H_2O. After 24 h, the oxidation rate of AISI 441 in 40% H_2O was about the same as in the other experiments.

Figure 3 shows the squared mass gain plotted against time. Except for AISI 441 in 40% H_2O, the parabolic rate law was followed by all samples, according to Eq. (2) where Δm is the change in mass, A is the total sample area, t is the exposure time, k_p is the parabolic oxide rate constant, and C is the integration constant that is dependent on the starting conditions [5]. If $\Delta m = 0$ at $t = 0$ then $C = 0$. The corresponding k_p values are given for the tested ferritic stainless steels in their respective exposure atmospheres in Table 3. If the initial rapid oxidation of AISI 441 in 40% H_2O is subtracted, it can be seen that parabolic oxidation proceeds after 24 h. This indicates that, after rapid oxidation at the start of the experiment, a protective oxide is established within the time period of 0-24 h.

$$\left(\frac{\Delta m}{A}\right)^2 = k_p t + C \qquad (2)$$

Table 3. k_p values from linear regression of parabolic plots.

AISI 441 - 10%	AISI 441 - 20%	AISI 441 - 40% - corrected	Crofer 22 APU - 10%	Crofer 22 APU - 20%	Crofer 22 APU - 40%
1.4E-13	1.4E-13	8.5E-14	1.2E-13	1.2E-13	1.2E-13

To investigate the different oxidation behavior of AISI 441 in 10-20% and 40% H_2O, cross sections of the oxide scale were prepared after 24 h and 500 h. The cross sections of AISI 441 after exposure to 10% H_2O are shown in Figure 4 as well as an EDX line scan across the oxide of the 24 h sample. The contrast in the oxide and the compositional EDX data show that the oxide consists of duplex layers, where the inner oxide is rich in Cr and the outer oxide contains both Cr and Mn. Figure 5 shows the XRD patterns from these two samples, from which it is possible to conclude that the oxide layer consists of inner corundum (Cr_2O_3) and outer spinel ($(Cr,Mn)_3O_4$). It can be seen in the micrographs that the majority of the oxide growth occurred in the chromia layer between 24 and 500 h. After 500 h, two crystal phases of Mn_3O_4 where identified by XRD: spinel phase and the tetragonal phase, hausmanntite. This is likely attributed to the outward diffusion of Mn, which is known to diffuse rapidly through chromia [20].

Figure 6 shows cross sections and EDX maps of AISI 441 samples exposed to 40% H_2O after 24 and 500 h. After 24 h, the oxide had become more uneven in thickness than the 10% H_2O sample. The oxide that formed in 40% H_2O had protrusions of seemingly outward-growing oxide distributed over the

surface and had thinner, flatter parts connecting the protrusions. Some of the protruding oxide was richer in Fe, but lacked oxygen, which indicates that these were originally Fe-rich oxides that were reduced during the ramp down and purging of the furnace. The other outer parts of the oxide contained about 2:1 Cr to Fe, but the inner part contained mostly Cr. Figure 7 shows XRD peaks from the AISI 441 samples exposed to 40% H_2O, and together with the information from EDX, it seems that the oxide is made of an inner layer of chromia and an outer layer of $(Cr,Fe)_3O_4$. The Si-EDX map in Figure 6 shows an interesting contrast. Enrichment of Si can be seen at the metal/oxide interface. A contrast in Si within the oxide scale can also be seen where there is more Si in the inner part than in the outer part of the oxide. This could be an indication that one part of the oxide, the Cr-rich part, grew inward and incorporated the existing Si of the alloy, and the more Fe-rich part grew outwards. This is in agreement with the work of Ardigo et al. who exposed AISI 441 at 800 °C to Ar- 1% H_2- 9% H_2O and found an oxide morphology similar to the one in the current study [14]. Using inert gold marker experiments as well as an isotope tracer experiment, those authors showed that the magnetite phase grew outward and the chromia grew inward. Figure 6 also shows that the Fe-rich protruding oxide has a thickness after 500 h similar to that after 24 h. Therefore it can be concluded that the Fe-rich spinel does not seem to have grown significantly after 24 h. In contrast, the Cr-rich oxide had increased in thickness. This is in good compliance with the mass gains in Figure 2 and would explain the reduction in oxidation rate after 24 h in the following way: Both Fe and Cr were initially oxidized and formed $(Cr,Fe)_3O_4$ with high ionic conductivity. After some limiting thickness was achieved, the inward flux of oxygen anions was sufficiently reduced for the enrichment of Cr at the metal/oxide interface. After this, a transformation to the corundum phase occurred, which has much lower ionic conductivity and a lower oxidation rate.

Figure 8 shows micrographs of cross sections of Crofer 22 APU after 500 h exposure to 10% and 40% H_2O. EDX (not shown here) shows that the inner part consisted of chromia and the outer part consisted of MnCr spinel. Some Mn-rich internal oxides beneath the chromia scale were also found, and these are expected to also have spinel crystal structure [22,23].

Parabolic kinetics for all samples after 24 h indicate diffusion-controlled oxidation. The similar kp values in 10%, 20% and 40% H_2O indicate that once a protective oxide is established, the ionic conductivity of the scale is similar in all environments. If the oxidation rate of the steel is governed by the growth of the slow-growing chromia scale, the similar kp values would indicate that there cannot be a significant difference in the defect concentration of the chromia in the different atmospheres. Thus, the results indicate that the dominating defect structure of the protective scale was governed by the pO_2, which was constant in all experiments here. However, several authors [18,24–26] have suggested that the dominant defect structure could be governed by the inner part of the oxide and therefore more dependent on the pO_2 at the metal/oxide interface than the pO_2 of the atmosphere. Or in other words, that oxidation rate has weak dependence on the pO_2 of the atmosphere. Therefore, the results could also be interpreted as a weak dependency of the defect chemistry of the protective scale on the change in absolute pressure of H_2/H_2O. Nevertheless, the similar oxidation rate constants in the differently diluted atmospheres indicate that formation of Fe-rich oxide, which was observed on AISI 441 in 40% H_2O, is not due to a difference in chromia defect chemistry. An alternative explanation for the rapid oxidation of FeCr alloys in steam has been suggested by Murata et al., who found that, after exposure of a Fe-10Cr alloy to steam at 750 °C, the major part of the hydrogen could be found in the $(Fe,Cr)_3O_4$. Those authors also measured the diffusivity of Fe in $(Fe,Cr)_3O_4$, with and without hydrogen, and found that hydrogen increased the rate of Fe diffusion dramatically. It is possible that the transition from unordered oxide to a protective oxide goes via a spinel phase ($(Fe,Cr)_3O_4$), and in the presence of hydrogen and water, this spinel is less protective. This causes a more rapidly growing $(Fe,Cr)_3O_4$ in 40% H_2O than in the more diluted atmospheres, which grows thicker before the inward flux of oxygen decreases sufficiently for a continuous chromia layer to be established. Thus, the crucial step for securing better corrosion resistance in H_2/H_2O environments could be the initial transient oxidation before continuous chromia formation. If this transient period is reduced, better long-term durability of the ferritic stainless steel could be expected

as a result. One method of improving the oxidation resistance has been presented by Ardigo et al. [27], who found that when samples of AISI 441 were polished and exposed to Ar- 1% H_2- 9% H_2O at 800 °C, protective chromia was formed, but when the steel was exposed in its as-rolled state more rapid oxidation with an outer $(Fe,Cr)_3O_4$ and inner $(Fe,Cr)_2O_3$ was observed. Those authors have explained this with a higher residual stress in the subsurface of the polished samples, which likely allows for faster Cr transport due to more dislocations.

5 Conclusions

The influence of the absolute pressure of H_2/H_2O at a constant pO_2 was investigated to better understand the mechanism of corrosion of ferritic stainless steel in simulated SOFC/SOEC fuel side environments. It was found that the oxidation rate of the steels and morphology of the formed oxides were almost identical regardless of the absolute pressure of H_2/H_2O for the Crofer 22 APU, and protective oxide behavior was seen for all the samples. The oxidation rate and morphology of the lower alloyed steel AISI 44 was similar to the oxidation rate and oxide morphology of Crofer 22 APU in 10-20% H_2O, however, no protective oxide layer was formed initially on AISI 441 in 40% H_2O. This led to rapid oxidation and the formation of $(Cr,Fe)_3O_4$. Thus, the dilution of a H_2/H_2O test atmosphere, compared to the real application, can lead to a change in the oxidation mechanism. It was shown here that the absolute pressure of H_2/H_2O is an important parameter for the selective oxidation of Cr in FeCr alloys.

6 Acknowledgements

The authors are grateful for funding by the Swedish Energy Agency (grant 2015-009652), the FFI program, as well as the Swedish High Temperature Corrosion Centre.

References

[1] J.W. Fergus, Metallic interconnects for solid oxide fuel cells, Mater. Sci. Eng. A. 397 (2005) 271–283. doi:10.1016/j.msea.2005.02.047.

[2] W.J. Quadakkers, J. Piron-Abellan, V. Shemet, L. Singheiser, Metallic interconnectors for solid oxide fuel cells – a review, Mater. High Temp. 20 (2003) 115–127. doi:10.3184/096034003782749071.

[3] M. a. Laguna-Bercero, Recent advances in high temperature electrolysis using solid oxide fuel cells: A review, J. Power Sources. 203 (2012) 4–16. doi:10.1016/j.jpowsour.2011.12.019.

[4] W.J. Quadakkers, J. Żurek, Oxidation in Steam and Steam/Hydrogen Environments, in: Shreir's Corros., 4th ed., Elsevier, 2010: pp. 407–456. doi:10.1016/B978-044452787-5.00022-6.

[5] P. Kofstad, High Temperature Corrosion, Elsevier Applied Science Publishers Ltd., New York, 1988.

[6] G. Hultquist, B. Tveten, E. Hörnlund, Hydrogen in Chromium: Influence on the High-Temperature Oxidation Kinetics in H2O, Oxide-Growth Mechanisms, and Scale Adherence, Oxid. Met. 54 (2000) 1–10. doi:10.1023/A:1004610626903.

[7] M. Hänsel, W.J. Quadakkers, D.J. Young, Role of Water Vapor in Chromia-Scale Growth at Low Oxygen Partial Pressure, Oxid. Met. 59 (2003) 285–301. doi:10.1023/A:1023040010859.

[8] J. Zurek, D.J. Young, E. Essuman, M. Hänsel, H.J. Penkalla, L. Niewolak, et al., Growth and adherence of chromia based surface scales on Ni-base alloys in high- and low-pO2 gases, Mater. Sci. Eng. A. 477 (2008) 259–270. doi:10.1016/j.msea.2007.05.035.

[9] S. Fontana, S. Chevalier, G. Caboche, Metallic interconnects for solid oxide fuel cell: Effect of water vapour on oxidation resistance of differently coated alloys, J. Power Sources. 193 (2009) 136–145. doi:10.1016/j.jpowsour.2008.11.041.

[10] P. Kofstad, On High Temperature Oxidation of Chromium, J. Electrochem. Soc. 127 (1980) 2410. doi:10.1149/1.2129481.

[11] A. Galerie, J.P. Petit, Y. Wouters, J. Mougin, A. Srisrual, P.Y. Hou, Water Vapour Effects on the Oxidation of Chromia-Forming Alloys, Mater. Sci. Forum. 696 (2011) 200–205. doi:10.4028/www.scientific.net/MSF.696.200.

[12] A. Holt, P. Kofstad, Electrical conductivity and defect structure of Cr2O3. II. Reduced temperatures (<∼1000°C), Solid State Ionics. 69 (1994) 137–143. doi:10.1016/0167-2738(94)90402-2.

[13] G. Bamba, Y. Wouters, A. Galerie, G. Borchardt, S. Shimada, O. Heintz, et al., Inverse growth transport in thermal chromia scales on Fe–15Cr steels in oxygen and in water vapour and its effect on scale adhesion, Scr. Mater. 57 (2007) 671–674. doi:10.1016/j.scriptamat.2007.06.050.

[14] M.R. Ardigo, I. Popa, S. Chevalier, S. Weber, O. Heintz, M. Vilasi, Effect of Water Vapor on the Oxidation Mechanisms of a Commercial Stainless Steel for Interconnect Application in High Temperature Water Vapor Electrolysis, Oxid. Met. 79 (2012) 495–505. doi:10.1007/s11085-012-9338-y.

[15] D. Caplan, G.I. Sproule, Effect of oxide grain structure on the high-temperature oxidation of Cr, Oxid. Met. 9 (1975) 459–472. doi:10.1007/BF00611694.

[16] E.W.A. Young, J.H. Gerretsen, J.H.. Wit, The oxygen partial pressure dependence of the defect structure of chromium(Ill)oxide, J. Electrochem. Soc. 134 (1987) 2257–2260.

[17] E.A. Polman, T. Fransen, P.J. Gellings, The reactive element effect; ionic processes of grain-boundary segregation and diffusion in chromium oxide scales, J. Phys. Condens. Matter. 1 (1989) 4497–4510. doi:10.1088/0953-8984/1/28/001.

[18] H. Kurokawa, Oxidation behavior of Fe–16Cr alloy interconnect for SOFC under hydrogen potential gradient, Solid State Ionics. 168 (2004) 13–21. doi:10.1016/j.ssi.2004.02.008.

[19] P. Alnegren, M. Sattari, J. Froitzheim, J.E. Svensson, Degradation of ferritic stainless steels under conditions used for solid oxide fuel cells and electrolyzers at varying oxygen pressures, Corros. Sci. 110 (2016) 200–212. doi:10.1016/j.corsci.2016.04.030.

[20] R.E. Lobnig, H.P. Schmidt, K. Hennesen, H.J. Grabke, Diffusion of cations in chromia layers grown on iron-base alloys, Oxid. Met. 37 (1992) 81–93. doi:10.1007/BF00665632.

[21] P. Alnegren, R. Sachitanand, M. Nikumaa, J. Grolig, H. Falk Windisch, M. Sattari, et al., Inhibiting chromium evaporation and oxide scale growth on SOFC metallic interconnects by nano coatings, 20th World Hydrog. Energy Conf. WHEC 2014. 1 (2014).

[22] M. Stanislowski, J. Froitzheim, L. Niewolak, W.J. Quadakkers, K. Hilpert, T. Markus, et al., Reduction of chromium vaporization from SOFC interconnectors by highly effective coatings, J. Power Sources. 164 (2007) 578–589. doi:10.1016/j.jpowsour.2006.08.013.

[23] H. Falk-Windisch, M. Sattari, J.-E. Svensson, J. Froitzheim, Chromium vaporization from mechanically deformed pre-coated interconnects in Solid Oxide Fuel Cells, J. Power Sources. 297 (2015) 217–223. doi:10.1016/j.jpowsour.2015.07.085.

[24] K.P. Lillerud, On High Temperature Oxidation of Chromium: I. Oxidation of Annealed, Thermally Ethced Chromium at 800 °-1100 °C, J. Electrochem. Soc. 127 (1980) 2397. doi:10.1149/1.2129478.

[25] P. Kofstad, K.P. Lillerud, On High Temperature Oxidation of Chromium: II. Properties of Cr2O3 and Oxidation Mechanism of Chromium, J. Electrochem. Soc. 127 (1980) 2410. doi:10.1149/1.2129481.

[26] T. Brylewski, Application of Fe–16Cr ferritic alloy to interconnector for a solid oxide fuel cell, Solid State Ionics. 143 (2001) 131–150. doi:10.1016/S0167-2738(01)00863-3.

[27] M.R. Ardigo-Besnard, I. Popa, O. Heintz, R. Chassagnon, M. Vilasi, F. Herbst, et al., Effect of surface finishing on the oxidation behaviour of a ferritic stainless steel, Appl. Surf. Sci. 412 (2017) 196–206. doi:10.1016/j.apsusc.2017.03.280.

7 Figures

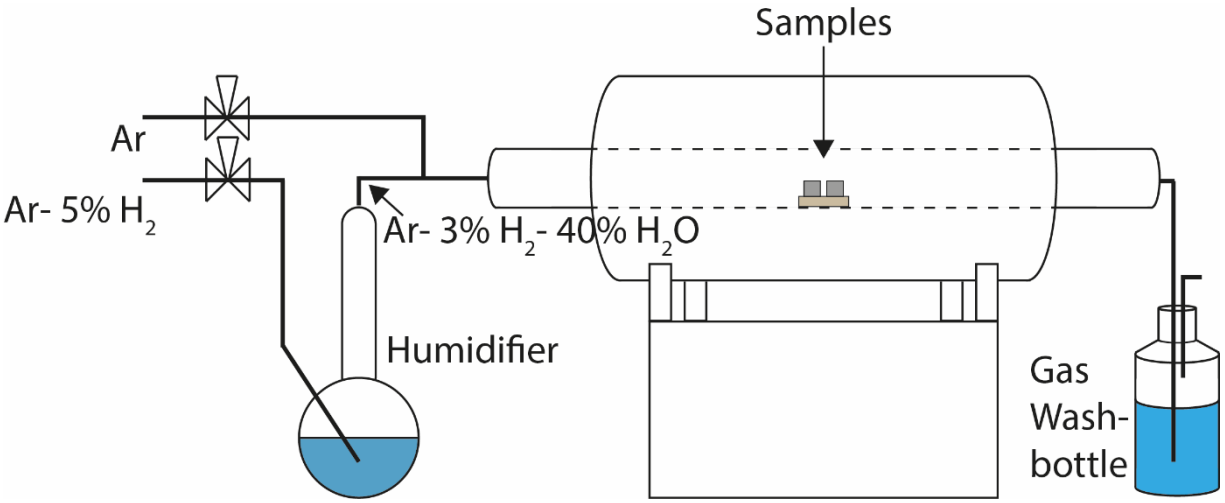

Figure 1. Schematic drawing of the experimental setup used.

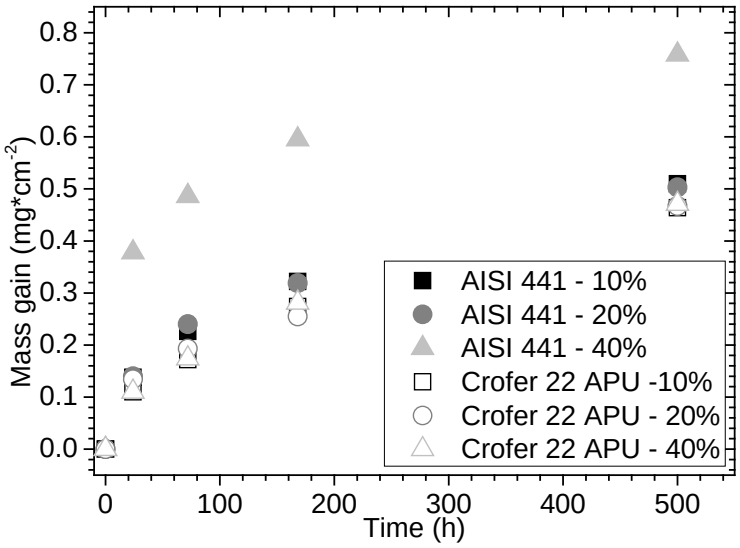

Figure 2. Mass gain plotted against time for AISI 441 and Crofer 22 APU in all tested atmospheres.

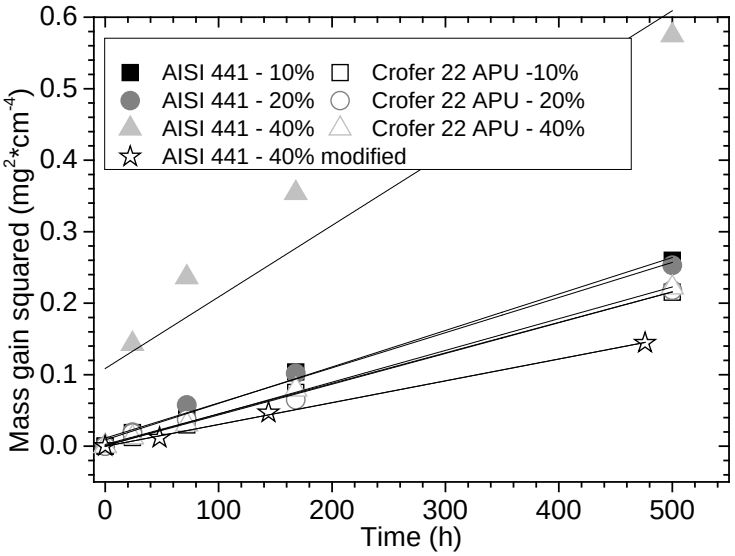

Figure 3. Mass gain squared plotted against time for AISI 441 and Crofer 22 APU in all tested atmospheres. The star-shaped data markers represent the mass gain of AISI 441 exposed to 40% H_2O, where the mass gain after the first 24 h of time was subtracted in order to evaluate if parabolic oxidation takes place after 24 h for AISI 441 in 40% H_2O.

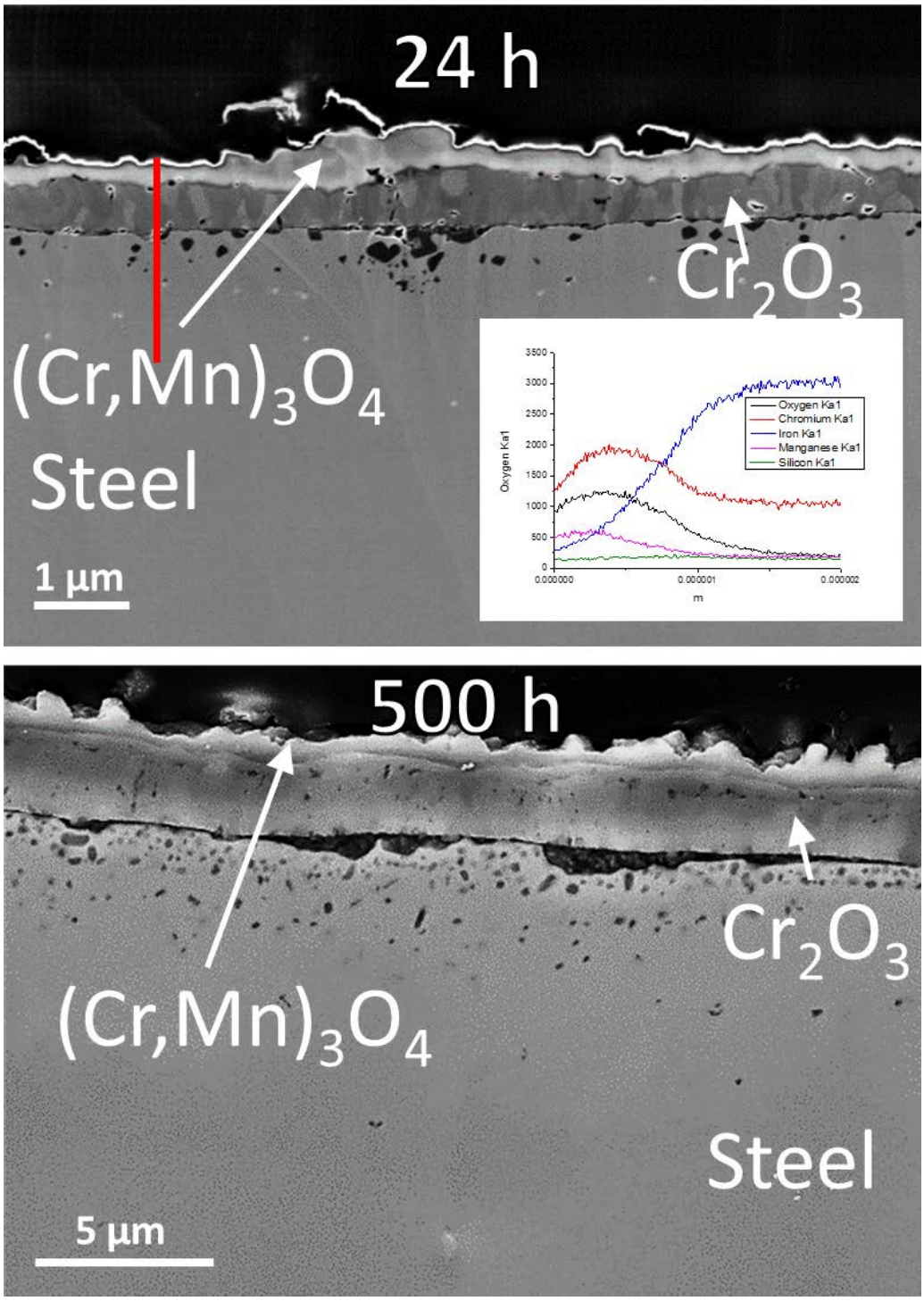

Figure 4. SEM micrographs of cross sections of AISI 441 exposed to 10% H_2O after 24 h (upper image) and 500 h (lower image). EDX line scan data is presented for the 24 h cross section, and the position of the line scan is indicated by a red line through the oxide in the upper image.

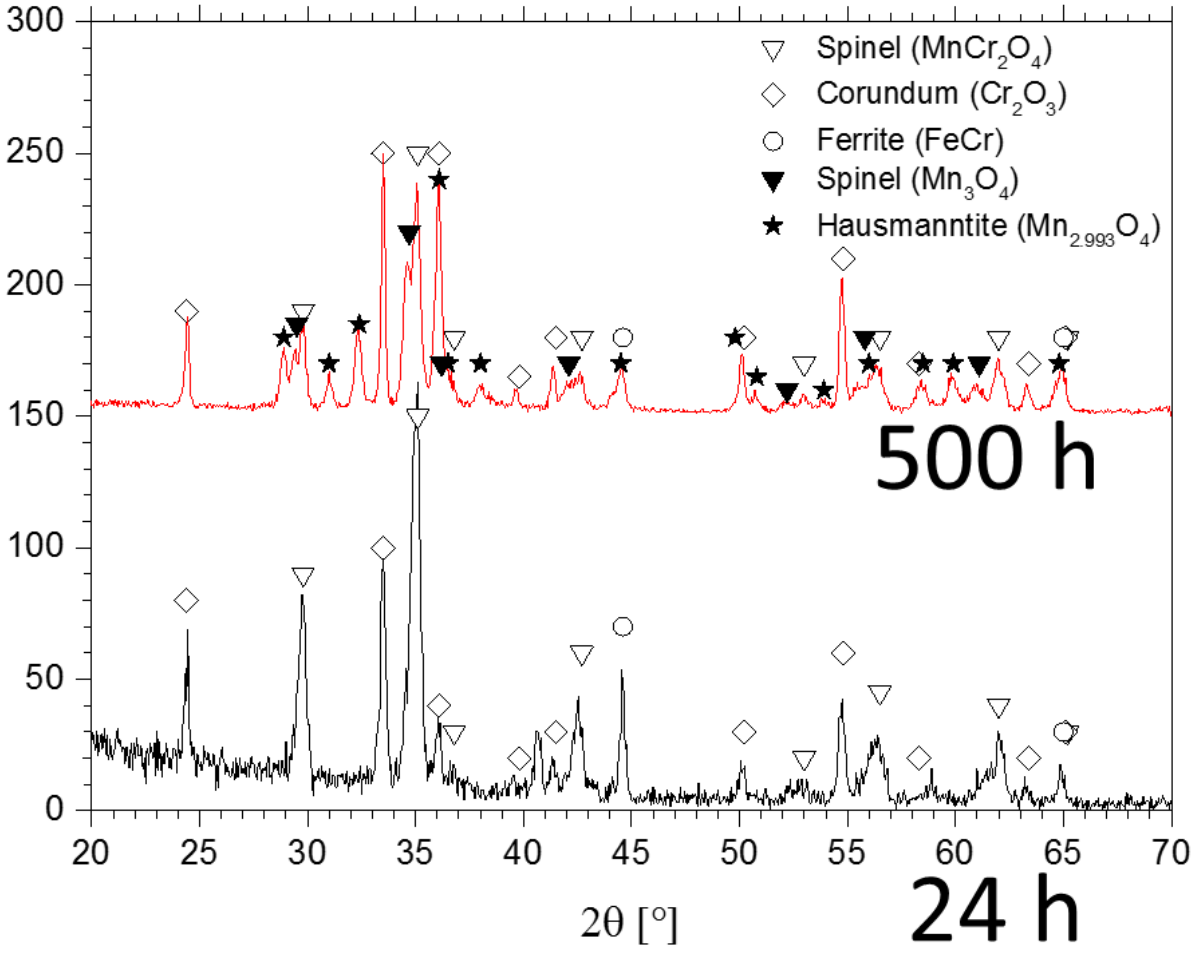

Figure 5. X-ray diffractogram of AISI 441 exposed to 10% H_2O after 24 h (lower spectrum) and 500 h (upper spectrum).

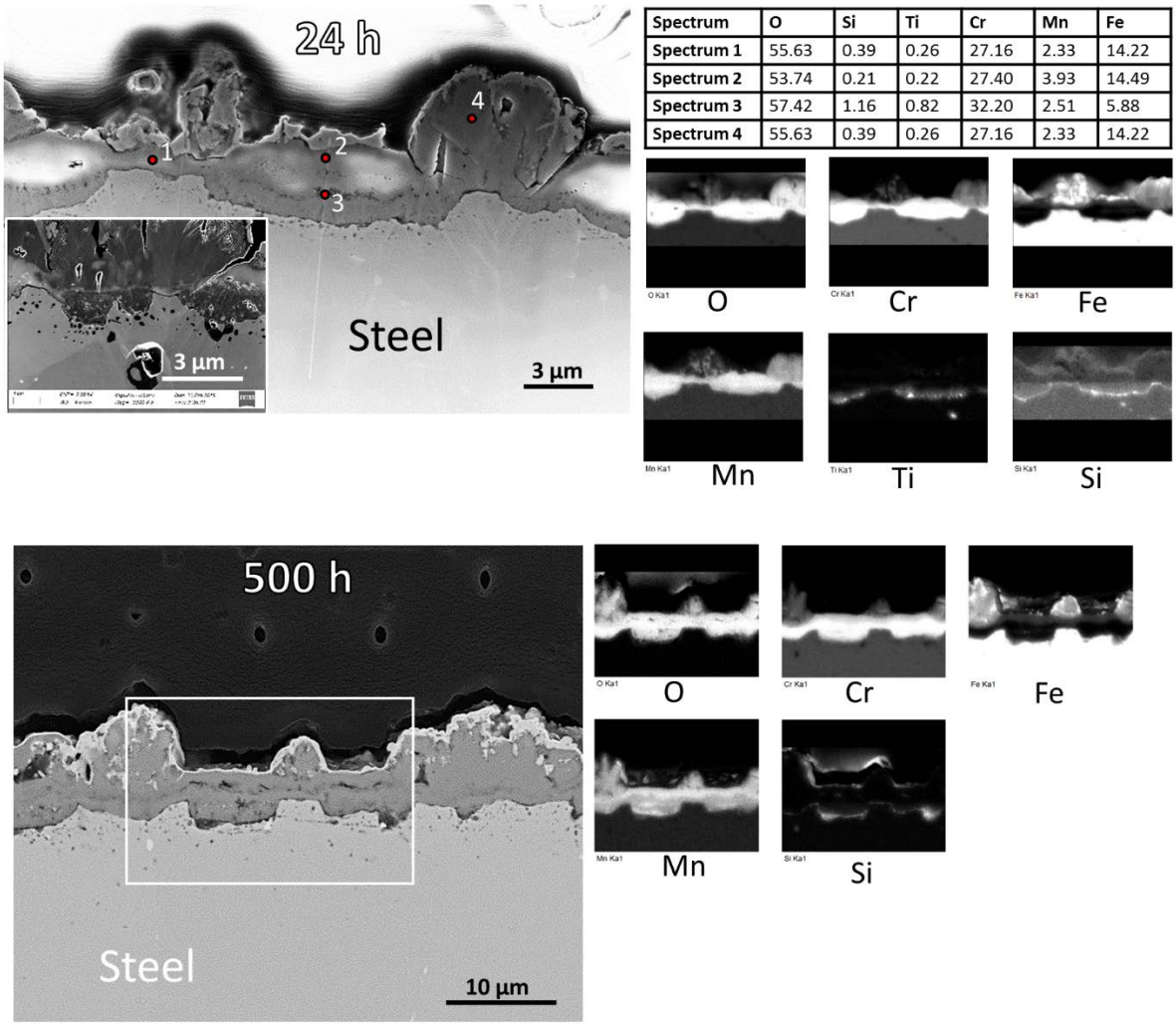

Spectrum	O	Si	Ti	Cr	Mn	Fe
Spectrum 1	55.63	0.39	0.26	27.16	2.33	14.22
Spectrum 2	53.74	0.21	0.22	27.40	3.93	14.49
Spectrum 3	57.42	1.16	0.82	32.20	2.51	5.88
Spectrum 4	55.63	0.39	0.26	27.16	2.33	14.22

Figure 6. SEM micrographs of cross sections of AISI 441 exposed to 40% H_2O after 24 h (upper image) and 500 h (lower image). EDX maps are given for both cross sections, and point analyses are given for the 24 h cross section, presented in atomic%, where the position is indicated by the numbered red dots. The position of the map analysis for the 500 h cross section is indicated by the white rectangle.

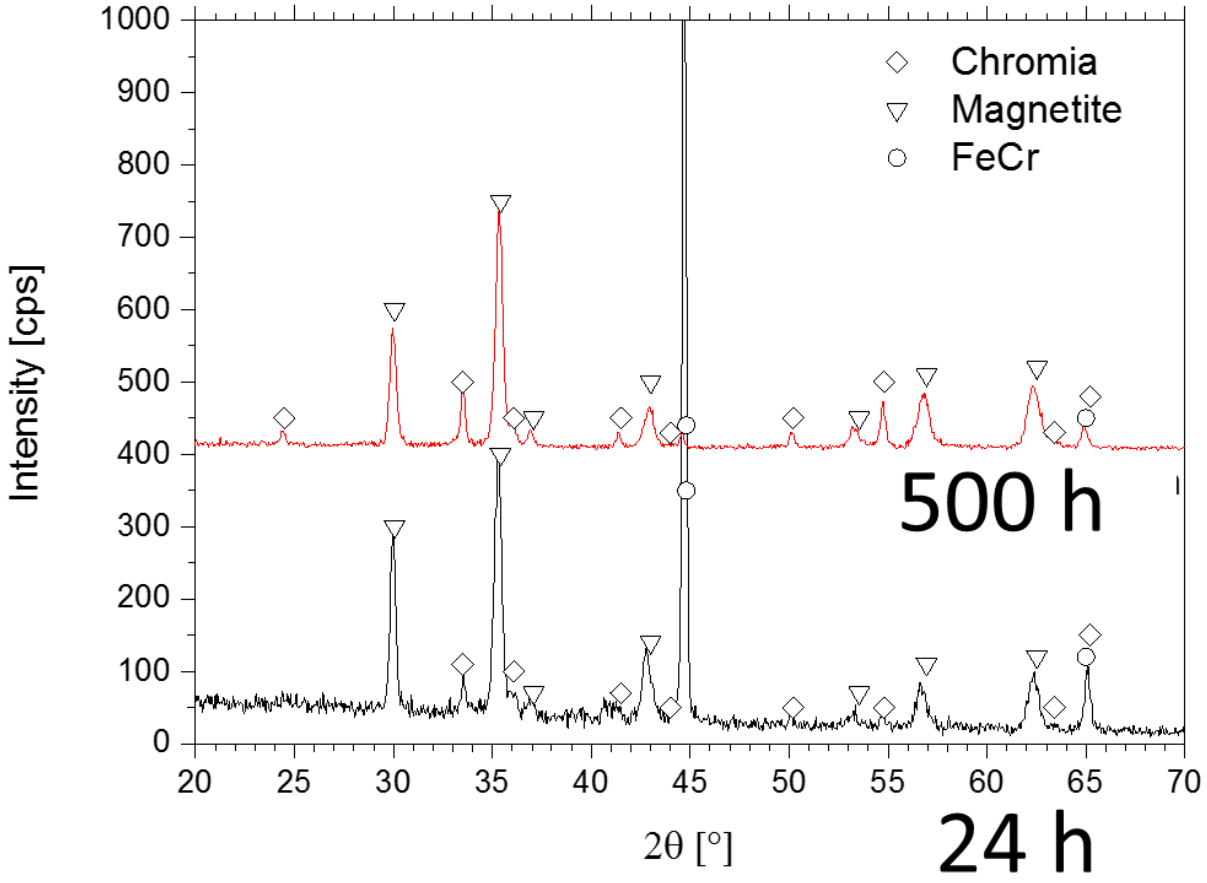

Figure 7. X-ray diffractogram of AISI 441 exposed to 4% H_2O after 24 h (lower spectrum) and 500 h (upper spectrum).

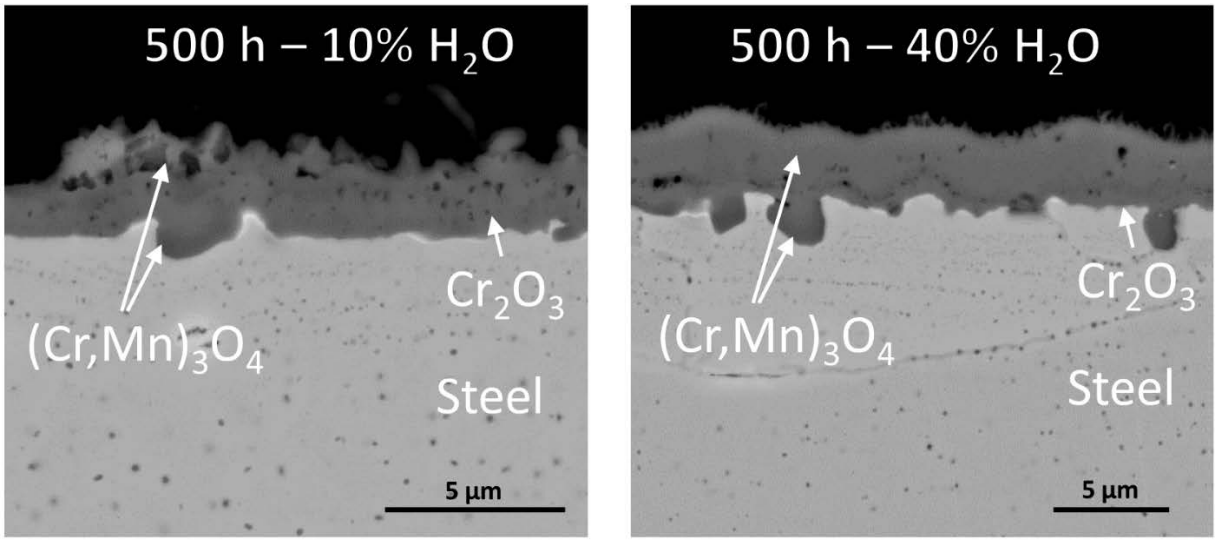

Figure 8. SEM micrographs of cross sections of Crofer 22 APU exposed to 10% H_2O after 500 h (left image) and 40% H_2O after 500 h (right image).